J Polym Res (2015) 22: 154
DOI 10.1007/s10965-015-0796-1

ORIGINAL PAPER

Investigation of perfluorinated proton exchange membranes prepared via a facile strategy of chemically combining poly(vinylphosphonic acid) with PVDF by means of poly(glycidyl methacrylate) grafts

Deniz Sinirlioglu[1] · **Ali Ekrem Muftuoglu**[2] · **Ayhan Bozkurt**[1,3]

Received: 27 April 2015 / Accepted: 7 July 2015 / Published online: 20 July 2015

Abstract A versatile and diverse grafting method was employed in the preparation of perfluorinated PEMs, in which poly(vinyl phosphonic acid) (PVPA) and poly(vinylidene fluoride) (PVDF) were chemically combined by means of poly(glycidyl methacrylate) (PGMA) grafts. Alkaline treated PVDF was used as a macromolecule in conjunction with GMA in the graft copolymerization. Various PVDF-*g*-PGMA-*g*-PVPA membranes were obtained upon simply mixing PVDF-*g*-PGMA and PVPA at several ratios by mass. The composition and the structure of the membranes were characterized by Energy Dispersive X-ray spectroscopy (EDS), ^{1}H-NMR, ^{19}F-NMR, and FTIR. Thermogravimetric analysis (TGA) demonstrated that the PVDF-*g*-PGMA and PVDF-*g*-PGMA-*g*-PVPA membranes were thermally stable up to 275 and 210 °C, respectively. The surface roughness and morphology of the membranes were studied using Atomic Force Microscopy (AFM), X-ray diffraction (XRD) and Scanning Electron Microscopy (SEM). The proton conductivity increased with increasing temperature and PVPA ratio in the absence of humidity. The maximum proton conductivity in anhydrous conditions at 150 °C was 0.0023 Scm^{-1} while in humidified conditions (under 50 % of RH) at 100 °C a value of 0.034 Scm^{-1} was found.

Keywords PVDF · Fuel cells · Poly(vinylphosphonic acid) · Alkaline treatment · Proton conductivity

Introduction

Recently, the development of proton exchange membranes (PEMs) has attracted significant interest among researchers since they play a critical role in the efficient operation of fuel cells by exchanging protons between anode and cathode [1–8]. The requirements for PEMs to be successfully employed in PEMFC include high proton conductivity, good mechanical properties, enhanced chemical stability, and low permeability [9–11]. At present, Nafion from DuPont, a good representative of perfluorosulfonic acid (PFSA) membranes, meets most of these criteria. Its molecular structure consists of polytetrafluoroethylene backbone and perfluorovinyl ether side chain bearing terminal sulfonic acid moieties. The backbone and the acid groups account for its excellent chemical stability and enhanced proton transport properties, respectively. Generally, Nafion exhibits an increasing trend in proton conductivity with increasing temperature. However, as temperature exceeds 80 °C, its proton conductivity decreases due to loss of water. This drawback of Nafion along with its high price, and low stability at high temperatures restrict the extent of its application and commercialization [6–8].

Keeping these considerations in mind, research efforts have been directed toward developing alternative membranes which are robust as Nafion and show high proton

Electronic supplementary material The online version of this article (doi:10.1007/s10965-015-0796-1) contains supplementary material, which is available to authorized users.

✉ Deniz Sinirlioglu
dsinirlioglu@fatih.edu.tr

✉ Ali Ekrem Muftuoglu
ekremm@yildiz.edu.tr

Ayhan Bozkurt
bozkurt@fatih.edu.tr

[1] Department of Chemistry, Faculty of Arts and Science, Fatih University, 34500 Buyukcekmece, Istanbul, Turkey

[2] Department of Chemical Engineering, Faculty of Chemical and Metallurgical Engineering, Yıldız Technical University, Davutpasa Campus, 34220 Esenler, Istanbul, Turkey

[3] Bio-nano Technology Center, Fatih University, 34500 Buyukcekmece, Istanbul, Turkey

conductivities. Sulfonated polymers, involving sulfonated poly(ether ether ketone) (SPEEK), sulfonated polysulfones (SPSU), sulfonated polyethersulfones, sulfonated polyetherketones, polybenzimidazole, have been synthesized as possible alternatives to Nafion [12–16]. Sulfonic acid groups ($-SO_3H$) have been situated in the polymer backbones more or less analogous to those of Nafion and were resposible for imparting hyhdrophilicity to the membranes easing the proton transporting ability. However, these as well possess the drawback of restricted proton conductivity at high temperatures [12–16].

Poly(vinylidene fluoride) (PVDF) based PEMs among others have shown some promising results as PVDF offers many favorable features such as durability, thermal stability and chemical resistance for efficient and prolonged operation of the fuel cell [10, 11, 17–21]. In their blends, the high hydrophobicity of PVDF might present some problems such as incompatibility with hydrophilic components and phase separation leading to disturbance in the proton transport mechanism [10, 11]. Therefore, homogeneous or surface grafting methods were more preferred to adopt hydrophilic nature to the PVDF membranes and maintain increased proton conductivity. In this respect, PVDF was grafted via various methods using UV light [19, 21, 22], gamma and X-ray irradiation [20, 23–26], ozone method, atom transfer radical polymerization (ATRP) [17, 27–32], and alkaline treatment [18, 33].

Various efforts to replace the water with less volatile proton conducting reagents have been made. In some anhydrous PEMs, phosphoric acid acted quite effectively as the proton source and solvent upon being doped in azole-functional polymer matrices [34–38]. At temperatures above 150 °C, the humidity gets low and the proton conductivities are typically high. However, at lower temperatures, due to high water uptake of the membranes, leaching out of the acid cannot be avoided. This situation presents apparent problems in prolonged usage of the cell. Poly(vinyl phosphonic acid) (PVPA) may be used as the phosphonated component because of its extremely high concentration of phosphonic acid directly attached to a flexible polymer main chain. The proton conductivity of pure PVPA homopolymer was reported as 1×10^{-3} S/cm under humid conditions [39, 40]. PVPA has a low Tg, which favors proton conductivity when copolymerized or blended with other rigid structures. On the other hand, PVPA as a homopolymer has poor film forming properties and the high acid concentration also makes it water-soluble. Therefore, it is important that PVPA be grafted to a more robust polymer such as PVDF.

Different synthetic grafting strategies, other than conventional ones, have to be necessarily developed in order to adjust the amount of poly(vinylphosphonic acid) immobilized on PVDF. It is well-known that "grafting from" and "grafting to" methods have restrictions in obtaining high grafting yields. Basically, the former requires the use of controlled / living polymerizations for tailoring the chain lengths while the latter is self-limiting, i.e., grafting sites cannot be fully exploited due to steric hindrance caused by the previously grafted chains.

Glycidyl methacrylate (GMA) is a useful monomer because the epoxy group can undergo ring opening reactions with various compounds. Polymers with epoxy groups can offer numerous functionalization possibilities [17, 29]. Previously, Aslan et al. reported the preparation of poly(vinyl phosphonic acid) grafted poly(glycidyl methacrylate), P(GMA)-*graft*-$P(VPA)_{10}$, which was simply a blending of the two homopolymers. The expected mechanism of grafting was the covalent linkage of the chains via the ring opening of epoxy with the proton of the acid. The membrane showed a maximum proton conductivity of 5×10^{-5} S/cm at 150 °C and under anhydrous conditions [41]. Thus, it seemed interesting to employ this approach in the production of perfluorinated PEMs, in which PVPA and PVDF were chemically combined by means of PGMA grafts.

In this contribution, a simple "grafting through" approach was employed in the preparation of PVDF-*g*-PGMA. Alkaline treated PVDF was used as a macromolecule along with glycidyl methacrylate (GMA) in the graft copolymerization. Upon the reaction of oxirane rings in the GMA side chains with PVPA, various PVDF-*g*-PGMA-*g*-PVPA membranes were fabricated. To the best of our knowledge, this is the first study to report the preparation of a PEM consisting of PVDF and PVPA. The composition and the structure of the graft copolymers were characterized by Energy Dispersive X-ray spectroscopy (EDS), ^{1}H-NMR, ^{19}F-NMR, and FTIR. Thermal properties were examined by thermogravimetric analysis (TGA) and differential scanning calorimetry (DSC). Besides, the morphology of the membranes was studied by X-ray diffraction (XRD), atomic force microscopy (AFM), and scanning electron microscopy (SEM). The electrochemical stability of the materials was tested by cyclic voltametry (CV). Proton conductivity of the PEMs both in anhydrous and humid conditions was investigated by dielectric-impedance analyzer.

Experimental

Materials

Polyvinylidene fluoride (PVDF, average Mw ~534,000) was purchased from Fluka. Glycidyl methacrylate (>99 %, Merck) was passed through basic alumina column to remove the inhibitor and stored at −20 °C. Azobisisobutyronitrile (AIBN; Merck) was recrystallized in THF prior to use. *N, N*-Dimethylformamide (DMF,≥99.9 %), methanol (99.9 %, Aldrich), potassium hydroxide (KOH, >85 %), and vinylphosphonic acid (>95 % Fluka) were used as received.

Preparation of PVDF-*g*-PGMA graft copolymer membranes

The synthetic approach of PVDF-*g*-PGMA copolymer is given in Fig. 1. The PVDF powder was first treated with potassium hydroxide (KOH). Briefly, PVDF was immersed in a 10 wt % KOH solution containing 0.05 wt % ethanol, and then the solution was stirred for 10 min at 60 °C. The precipitate was collected by filtration and then washed with distilled water.

A 5 g sample of alkaline-treated PVDF powder was dissolved in 60 mL of *N,N*-dimethylfomamide (DMF) at 70 °C. After the complete dissolution, the monomer GMA (5 mL, 5.35 g) and 0.1235 g of AIBN (2 % mol) were added to the system under a N_2 atmosphere with continuous magnetic stirring. The graft polymerization proceeded in an oil bath for 24 h at 70 °C. The obtained graft copolymer (PVDF-*g*-PGMA) was precipitated by excess methanol, then filtrated, and washed thoroughly with excess chloroform for 24 h to remove the PGMA homopolymers. All samples were dried in vacuum oven for 2 days at 70 °C.

Preparation of PVDF-*g*-PGMA-*g*-PVPA(x) membranes

Poly(vinyl phosphonic acid) (PVPA) was produced by free radical polymerization of vinyl phosphonic acid as discussed in an earlier study [42]. PVDF-*g*-PGMA and PVPA were dissolved in DMF and water, respectively. Stoichiometric amounts of PVDF-*g*-PGMA and PVPA solutions (PVDF-*g*-PGMA-*g*-PVPA(x)); x=5, x=10, x=20 were admixed. For instance, to obtain PVDF-*g*-PGMA-*g*-PVPA(20), 0.5 g PVDF-*g*-PGMA in 40 mL DMF and 0.1 g PVPA in 0.4 mL water were mixed and stirred for 24 h at 70 °C. The graft samples, PVDF-*g*-PGMA-*g*-PVPA(x) were precipitated in diethyl ether and purified by washing with methanol and distilled water, respectively, to remove unreacted PVPA. The obtained graft copolymers are soluble in DMF and the solutions of the samples were cast in polished polytetrafluoroethylene plates. The solvent was evaporated in vacuum oven at 60 °C. Free-standing films were obtained and stored in the glove box during characterizations.

Characterization

Fourier transform infrared spectroscopy (FTIR) FT-IR spectra were recorded using a Bruker Alpha-P in ATR in the range of 4000–400 cm^{-1}.

NMR spectroscopy ^{1}H-NMR and ^{19}F-NMR spectra were recorded using a 400 MHz Bruker Avance spectrometer. Chemical shifts were reported in ppm relative to TMS as internal standard.

Thermogravimetric Analysis (TGA) Thermal stabilities of the membranes were analyzed by a Perkin Elmer STA 6000 Thermal Analyzer. The samples (~10 mg) were heated between 30 and 750 °C under N_2 atmosphere at a scanning rate of 10 °C/min.

Differential Scanning Calorimetry (DSC) Perkin Elmer JADE Differential Scanning Calorimetry (DSC) was used to investigate the thermal transitions of the samples. The samples

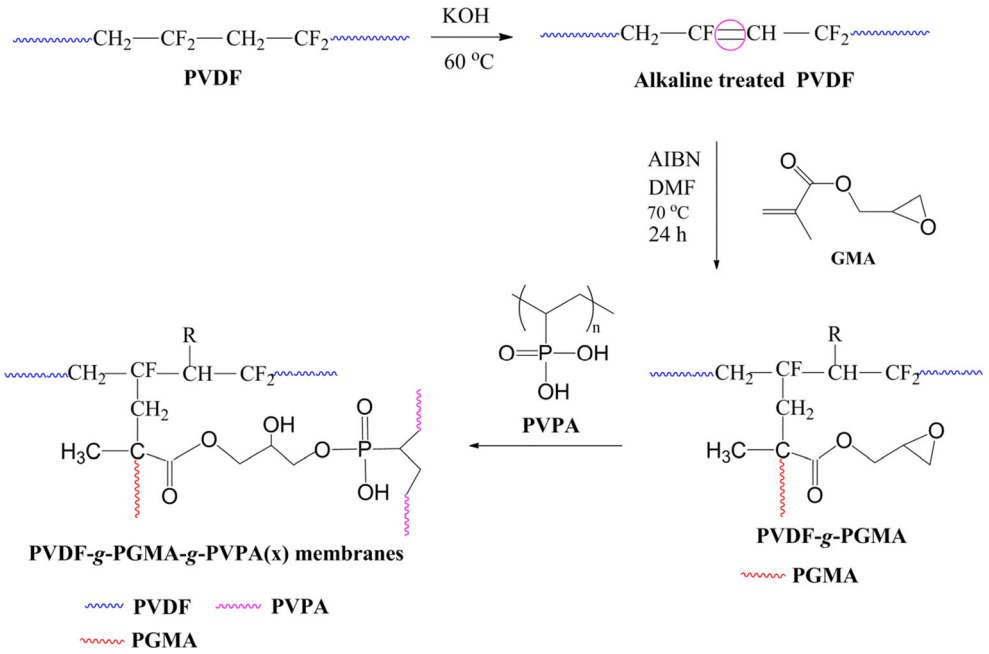

Fig. 1 Schematic illustration for the PVDF-*g*-PGMA copolymer synthesis and PVDF-*g*-PGMA-*g*-PVPA(x) membrane formation

(~10 mg) were put into aluminum pans. In heat flux instruments, the sample and reference are heated from the same source and the temperature difference is measured. During the measurements, firstly the samples were heated from −50 to 150 °C, and then they were cooled from 150 to 0 °C. Finally, the second heating was performed from 0 to 250 °C at a rate of 10 °C/min under nitrogen atmosphere.

Scanning electron microscopy The surface morphology of the membranes was determined by using a scanning electron microscopy (SEM) type JEOL-7001 FESEM (Tokyo, Japan) instrument. All of the samples were previously coated with gold for 150 s in a sputtering device.

Atomic force microscopy The tapping mode AFM images of the PVDF, PVDF-*g*-PGMA, and PVDF-*g*-PGMA-*g*-PVPA(x) membranes were acquired using a Park AFM (XE-100, Park AFM, Korea), supported on a Minus-K (25BM-6, Minus-K, Inglewood, CA) vibration isolation base. The AFM parameters to obtain the images were carefully set to minimize the pressure of tip on the composite membranes. 10×10 μm images were acquired at a resolution of 512×512 points within the range of 0.5–0.8 Hz scan rate and were subjected to first-order flattening. Surface roughness was calculated by using the Root Mean Square (RMS), that is, the standard deviation of the Z values within a given area, defined by the following equation:

$$\mathrm{RMS} = \sqrt{\frac{\sum_{i=1}^{N}(Z_i - Z_{ave})^2}{N}} \quad (1)$$

where Z_{ave} is the average, Z_i is the current Z value, and N is the number of points within the analyzed area. It was noted that the surface roughness depends on the curvature and size of the AFM tip and on the image processing. The RMS mean values and the standard deviations were obtained by analyzing at least 8 AFM images.

Water uptake measurements Water uptake (WU) measurement was carried out by the weight difference between the fully hydrated membranes and dried membranes. The dried membranes (W_{dry}) were weighed and then wetted until the weight remained constant. The wet or saturated weights of the membranes (W_{wet}) were measured quickly after removing or wiping out any remaining surface water with a paper. The water uptake was calculated according to the formula (1):

$$WU(\%) = \frac{Wwet - Wdry}{Wdry} \times 100 \quad (2)$$

Methanol permeability measurements Methanol permeability was measured using our homemade diaphragm diffusion cell with a volume of 4 mL. The cell was filled with a pure methanol. Methanol vapor in equilibrium with the liquid diffused along the concentration gradient through the membrane, which was clamped between the mouth of glass and the cap. The cap has a hole with a 0.82 cm diameter so that the methanol diffused through the membrane could escape. The weight loss was recorded as a function of time and the data were used for permeability calculations.

X-ray powder diffraction (XRD) X-ray powder diffraction (XRD) patterns of PVDF, PVDF-*g*-PGMA, and PVDF-*g*-PGMA-*g*-PVPA(x) membranes were determined by using X-ray diffraction instrument, Rigaku Smart Lab Diffractometer, operated at 40 kV and 35 mA using Cu Ka radiation. The XRD peaks were recorded in the 2θ range of 10°–70°.

Cyclic voltammetry Cyclic voltammograms were obtained with a potentiostat CHI instrument Model 842B. Voltammograms of all membranes were recorded in a three electrode CV system, using a polymer electrolyte modified Pt working electrode and a Pt counter electrode. The reference electrode was silver/silver chloride (Ag/AgCl) calibrated by a ferrocene/ferricinium redox system. Cyclic voltammetry studies were carried out in 0.1 M tetraethylammonium chloride (TBACl)/acetonitrile.

Proton conductivity measurements The proton conductivity measurements were performed using a Novocontrol dielectric-impedance analyzer. The proton conductivities of the PVPA homopolymer, PVDF-*g*-PGMA graft copolymer, and PVDF-*g*-PGMA-g-PVPA(x) (x=5.0, 10.0, and 20.0) membranes were measured between 20 and 150 °C. All membranes were fixed between additional external parallel plate electrodes (between platinium blocking electrodes) to make a sandwich using the simple two-electrode method and impedance was measured by varying the temperature from 20 to 150 °C and the proton conductivities were measured in 1 Hz and 3 MHz frequency range at 10 °C intervals. The temperature was controlled with a Novocontrol cryosystem, which is applicable between −150 and 250 °C.

Results and discussion

PVDF-*g*-PGMA was synthesized via free radical-initiated graft copolymerization of glycidyl methacrylate (GMA) from alkaline-treated PVDF backbone, followed by the reaction of oxirane rings in the GMA side chains with poly(vinyl phosphonic acid) (PVPA). Various PVDF-*g*-PGMA-*g*-PVPA(x) membranes were thus obtained as depicted in Fig. 1. Free-standing film was obtained. (please see the Supporting Information, Figure S1).

The critical concern associated with grafting via alkaline treatment of PVDF is whether the alkaline treatment actually produces double bonds and that the GMA units polymerize through these bonds forming PVDF-*g*-PGMA. Previously, Ross et al. reported a detailed study on surface modification of PVDF by alkaline treatment [43]. They investigated the possibility of both defluorination and oxygenation and proposed a degradation mechanism. They were able to prove the formation of conjugated double bond structures by using ToF-SIMS (time-of-flight secondary ion mass spectroscopy), XPS (X-ray photoelectron spectroscopy), Raman spectroscopy, and FT-IR. In the present work, we have determined considerable spectroscopic evidence for double bond formation on PVDF upon treatment. These will be discussed below. Furthermore, it can well be expected that the "Grafting Through" strategy works under these conditions, that is, the double bonds situated on PVDF backbone contributes to propagation. The reason is that spectroscopic evidence attributed to PGMA to be discussed below can not originate from homopolymer formation since it is expected that all the possibly formed homopolymer must have been removed upon thorough washing with excess chloroform for 24 h.

The composition of PVDF-*g*-PGMA was determined by EDS analysis and the results are summarized in Table 1, which were well supported by C, F, and O content calculated in conjunction with grafting degree (GD) obtained from ^{1}H-NMR.

FTIR analysis

To provide evidences for grafting PGMA and PVPA, FTIR analysis was performed on the membrane in comparison with PGMA, PVDF and alkaline treated PVDF homopolymers, and PGMA-grafted films as shown in the FTIR spectra are represented in Fig. 2. In PGMA, the carbonyl group gives a strong peak at 1725 cm^{-1} and the strong peaks at 1140 and 1260 cm^{-1} are attributed to C-O stretching of the ester group. The absorption peak at 906 cm^{-1} belongs to epoxy (oxirane) rings (Fig. 2a). The spectrum of PVDF film exhibited a number of strong bands in the range of 1000–1370 cm^{-1} representing CF_2 groups, in addition to, a small band between at 3024 and 2982 cm^{-1} representing stretching vibrations of -CH_2 groups [17–19, 21]. Degradation of PVDF was performed by alkaline treatment (defluorination due to alkaline treatment leading to the introduction of hydroxyl and carbonyl groups) [33, 43]. FTIR spectra of alkaline treated PVDF (Fig. 2c) show that the broad absorption peaks between 3600 and 3000 cm^{-1} might be due to H-bonded -OH groups while those between 1740 and 1600 cm^{-1} can be associated with the strecthing vibrations of C=O and C=C groups in different molecular frames [18, 33, 43–45]. Differing from that of the alkaline treated PVDF homopolymer, the grafted films, PVDF-*g*-PGMA, showed additional characteristic bands in the at 1735 cm^{-1}, attributable to the ester stretching

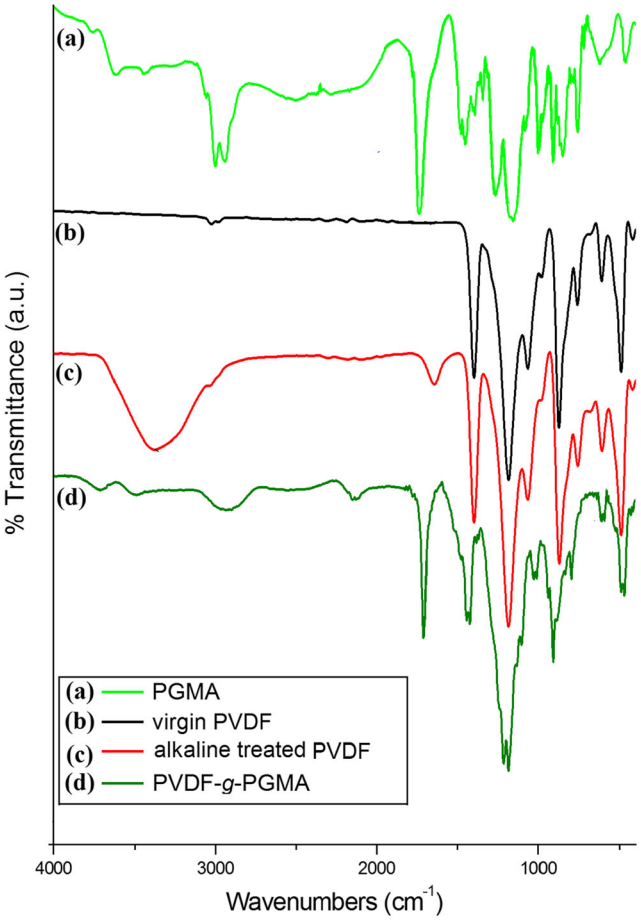

Fig. 2 FTIR spectra of (**a**) PGMA, (**b**) virgin PVDF, (**c**) alkaline treated PVDF and (**d**) PVDF-*g*-PGMA

Table 1 Chemical compositions of PVDF-*g*-PGMA graft copolymer

	Sample	Grafting degree (%)[a]	Grafting degree (%)[b]	Chemical elements (%)[c]		
				C	F	O
Theoretical	PVDF-*g*-PGMA	–	–	46.01	33.51	15.02
Found	PVDF-*g*-PGMA	36.30	80.62	49.62	32.91	15.19

[a] found from ^{1}H-NMR on a % by mol basis

[b] found from ^{1}H-NMR on a % by weight basis

[c] found from EDS results on a % by weight basis

mode of the grafted GMA segments. The bands at 2800–3000 cm^{-1} were assigned for C-H of the grafted GMA. Furthermore, PVDF-*g*-PGMA shows the absorption at 903 cm^{-1} which is assigned to strecthing vibration of the epoxy group [46]. The strong peaks at 1257 and 1143 cm^{-1} are attributed to C-O strecthing of the ester group [17]. Furthermore, disappearance of the relatively broad peak at 1649 cm^{-1} corresponding to carbon-carbon double bond indicates that PGMA has been grafted through PVDF upon rupture of C=C double bond during polymerization (Fig. 2d).

Figure 3 shows the FTIR spectra of PVPA homopolymer, PVDF-*g*-PGMA, and PVDF-*g*-PGMA-*g*-PVPA membranes, respectively. Pure PVPA has strong bands at 990 and 910 cm^{-1} that belong to asymmetric stretching vibrations of the P-OH group and at 1150 cm^{-1} that corresponds to P=O stretching [5]. The C=C band of the vinyl phosphonic acid

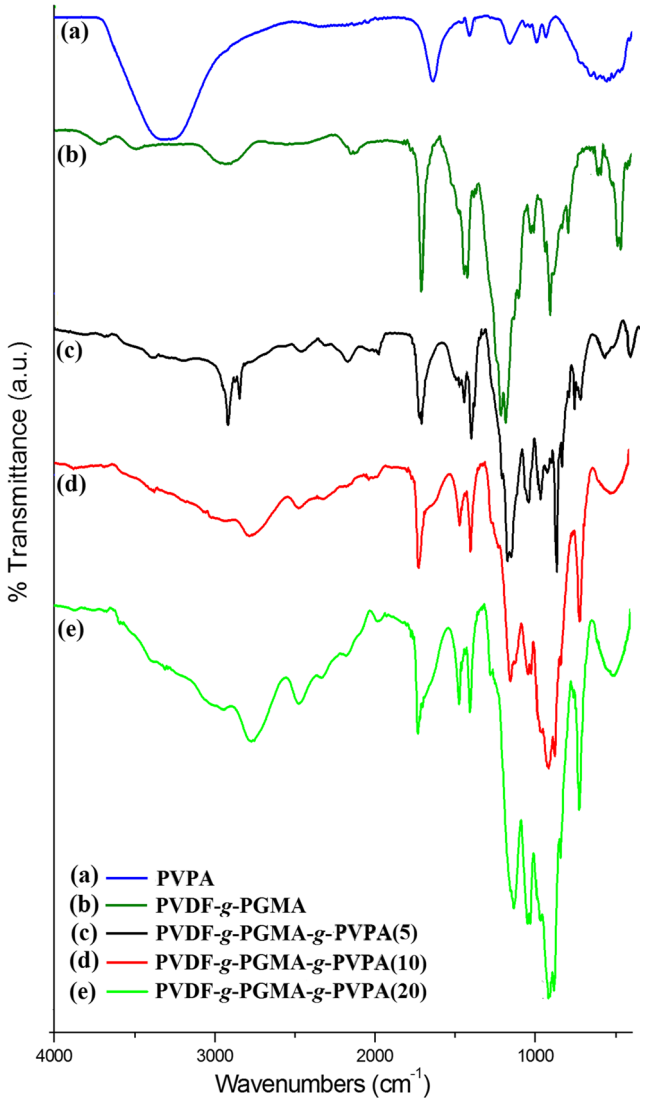

Fig. 3 FTIR spectra of (**a**) PVPA, (**b**) PVDF-*g*-PGMA, (**c**) PVDF-*g*-PGMA-*g*-PVPA(5), (**d**) PVDF-*g*-PGMA-*g*-PVPA(10), and (**e**) PVDF-*g*-PGMA-*g*-PVPA(20)

was evident at 1635 cm^{-1}. Peaks associated with -CH stretchings were observed in the vinyl phosphonic acid between 2800 and 3000 cm^{-1}. In the PVPA grafted PVDF-*g*-PGMA membranes, at higher VPA ratio (Fig. 3e), the P-O-H vibration at 930 cm^{-1} becomes stronger, indicating the existence of excess acidic protons. The intensity of these peaks increased in parallel with the concentration of PVPA into the grafted membranes. These peaks are overlapped with the corresponding peaks of PVDF units of grafted-matrix and became broader (Fig. 3c-e). Furthermore, the band broadening between 3500 and 2000 cm^{-1} is due to the hydrogen bonding network between epoxy groups of PGMA and phosphonic acid units of PVPA which is necessary for proton conduction [5, 41]. These signs evidenced that PVPA was immobilized onto PVDF-*g*-PGMA.

^{1}H-NMR analysis

The successful graft copolymerization was confirmed using ^{1}H-NMR and ^{19}F-NMR spectroscopy. Figure 4 shows ^{1}H-NMR spectra of alkaline treated PVDF and PVDF-*g*-PGMA. For all samples, the peaks of solvent (DMSO) and water appeared at 2.51 and 3.37 ppm, respectively. The ^{1}H-NMR spectrum exhibited the characteristic multiplets centered at 2.91 and 2.28 ppm originating from the methylene groups in -CH_2-CF_2-**CH_2**-CF_2-CH_2-CF_2- and -CF_2-**CH_2**-**CH_2**-CF_2- sequences appearing in the normal head-to-tail (ht) and reversed tail-to-tail (tt) VDF additions [17–19]. The new multiple peaks at 6.0–6.5 ppm in alkaline treated PVDF correspond to the protons on the double bonds (−CH_2-CF=**CH**-CF_2-) after the elimination of HF from PVDF [47–50]. These peaks evidenced the formation of the double bonds (−CH_2-CF=**CH**-CF_2-) in the alkaline treated PVDF. The methylene groups of PGMA backbone exhibited signals at 1.89 and 1.82 ppm (b). The signals observed at 0.98 and 0.81 ppm (c) are due to the protons in the -CH_3 groups of PGMA. The spectrum also indicated two signals at 4.35 and 3.75 ppm (d), attributable to -$COOCH_2$- group of PGMA. The peaks at 3.25 ppm (e), 2.8 and 2.66 ppm (f) are due to the protons of the oxirane ring [17, 29]. In addition, the signals at 2.75, 2.89 and 7.99 ppm belong to the dimethylformamide (DMF).

The successfully introduced double bond in the PVDF could also be confirmed by ^{19}F-NMR. The spectra of PVDF, alkaline treated PVDF, and PVDF-*g*-PGMA graft copolymer are shown in Fig. 5. The structure of PVDF is dominated by the presence of VDF-VDF head-to-tail (ht) (−CH_2-CF_2-CH_2-CF_2-CH_2-CF_2-) sequences appearing between −92 and −96 ppm, and VDF-VDF tail-to-tail (tt) (−CF_2-CH_2-CH_2-CF_2-) structure appearing between −114 and −117 ppm [47, 48, 51]. Compared with PVDF, the new signals emerging at around −107 ppm in alkalined treated PVDF could be assigned to the F atoms in the double bond (−CH_2-CF=CH-CF_2-) units [47, 48, 52]. The same peaks at around −107 ppm

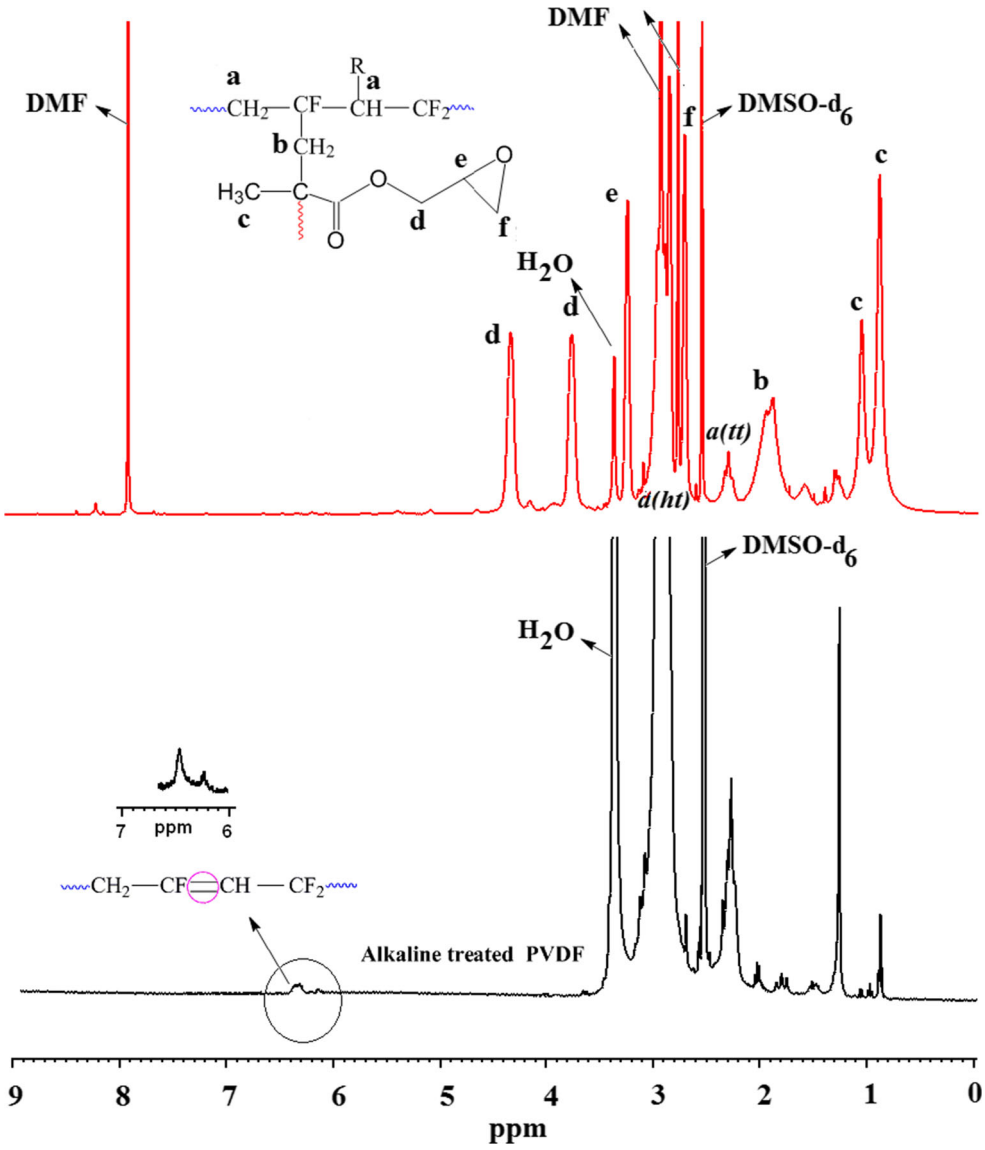

Fig. 4 ^{1}H-NMR spectra of alkaline treated PVDF and PVDF-*g*-PGMA graft copolymer recorded in DMSO-d_6

were also detectable in the spectrum of PVDF-*g*-PGMA (in Fig. 5), supporting that grafting has successfully occurred. It is also noteworthy that signals attributed to PGMA can not originate from homopolymer formation since it is expected that all the possibly formed homopolymer must have been removed upon thorough washing with excess chloroform for 24 h as previously mentioned.

The integration ratio of the protons in the ^{1}H-NMR yielded a degree of grafting of 80.62 % using the following Eq. (2):

$$\text{Degree of Graftiing(GD)}(\%) = \frac{\text{Mw}_{(\text{glycidyl methacrylate})} \times \text{A(d + d)}}{\text{Mw}_{(\text{PVDF})} \times \text{A(a)}} \times 100 \quad (3)$$

where Mw(PVDF) is molecular weight of repeating unit of PVDF, A(a) are the integral areas of the characteristic peak (a) of the PVDF main chain (used as reference peak) and -CH_2 protons of the glycidyl methacrylate (d) of PGMA, respectively.

Thermal analysis

Prior to the analysis, the membranes were dried under vacuum at 100 °C for 24 h and stored in a glove box. The DSC measurements were carried out under inert atmosphere at a scan rate of 10 °C/min and the second heating curves were evaluated. DSC thermograms of the original PVDF, PVDF-*g*-PGMA, and PVDF-*g*-PGMA-*g*-PVPA(x) membranes are given in Fig. 6. Previously, pure PVPA was reported to have a T_g of −23 °C [53, 54]. The glass transition temperature (T_g) of the PGMA homopolymer and original PVDF were studied as 74 °C [46, 55] and −50 °C [56], respectively. PVDF-*g*-PGMA displayed a glass transition at approximately

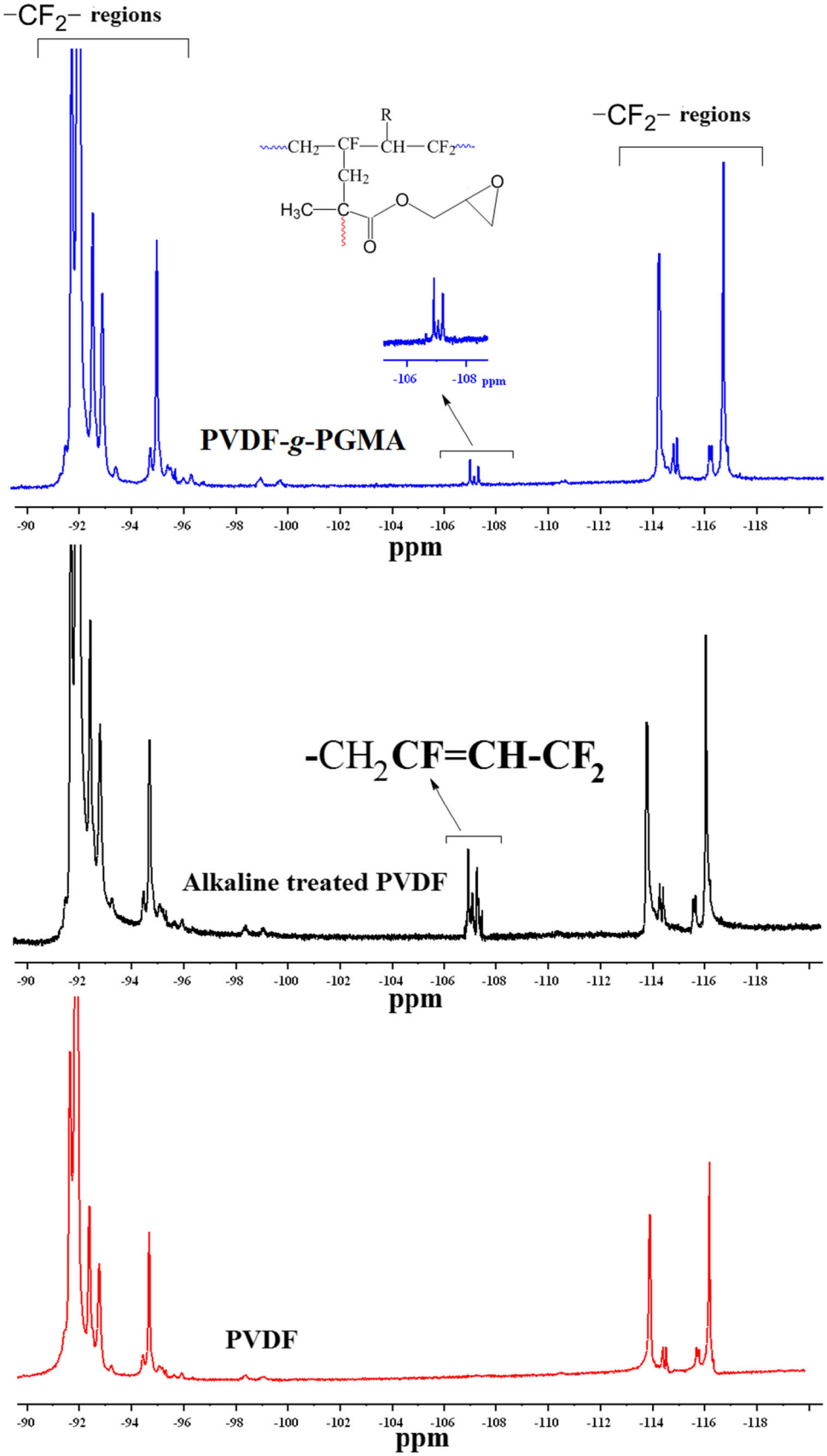

Fig. 5 ^{19}F-NMR spectra of PVDF, alkaline treated PVDF, and PVDF-*g*-PGMA graft copolymer recorded in DMSO-d_6

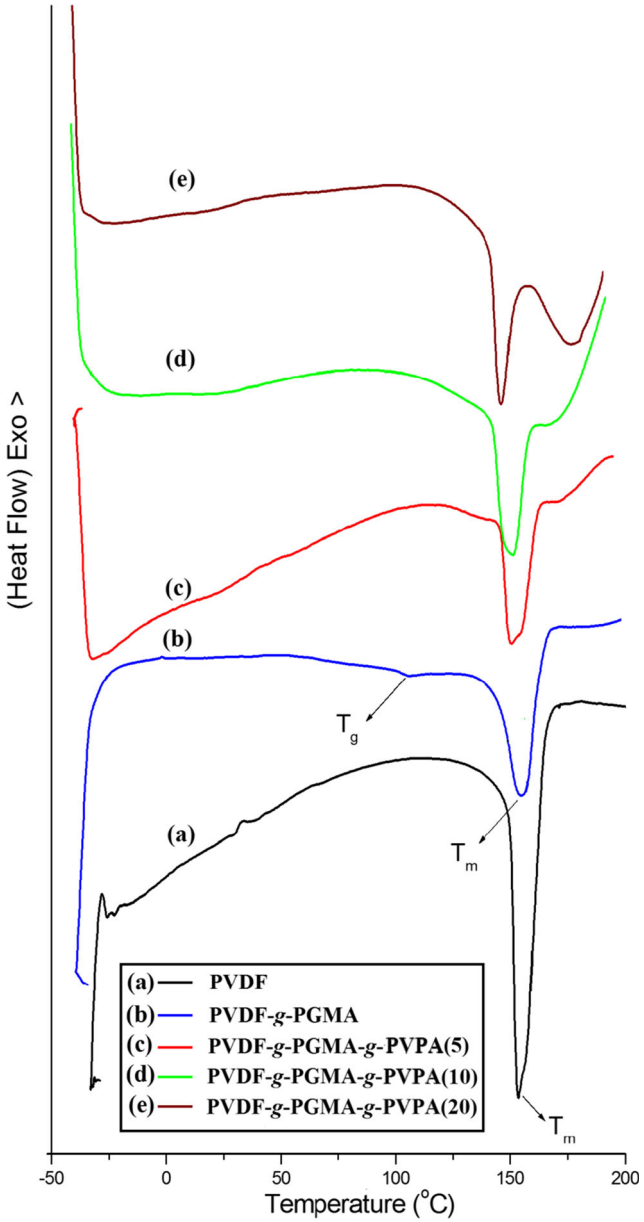

Fig. 6 DSC thermograms of (**a**) original PVDF, (**b**) PVDF-*g*-PGMA, (**c**) PVDF-*g*-PGMA-*g*-PVPA(5), (**d**) PVDF-*g*-PGMA-*g*-PVPA(10), (**e**) PVDF-*g*-PGMA-*g*-PVPA(20) membranes recorded under N_2 atmosphere at a heating rate of 10 °C/min

106.8 °C. The melting point (T_m) was observed at approximately 157.2 °C due to the presence of ordered PVDF regions. For PVDF-*g*-PGMA-*g*-PVPA(x) membranes, a T_g might have been observed between 106.8 and −23 °C, however, no T_g could be detected. They only demonstrated melting points (T_m) at approximately 156.5, 156.1 and 155.6 °C, respectively (Fig. 6). The lessening in the melting point could be considerably decrease of the crystalline region of PVDF-*g*-PGMA with the amorphous PVPA grafts.

The thermal stability of the membranes was analyzed with TGA in comparison with the PVDF, PVDF-*g*-PGMA, and PVDF-*g*-PGMA-*g*-PVPA(x) proton conducting membranes and the obtained TGA curves are represented in Fig. 7. Pristine homopolymer, PGMA, was reported to be thermally stable up to 200 °C [46]. PVPA homopolymer is thermally stable until 200 °C but there is a little weight loss between 100 and 200 °C due to condensation of phosphonic acid units [3, 5, 8]. The original PVDF film showed a single-step degradation pattern with transition at about 460 °C due to the decomposition of molecular chains of PVDF [17–19, 21], whereas the PGMA grafted PVDF film showed a two-step degradation pattern at 275 and 460 °C due to the decomposition of PGMA grafts and the PVDF matrix, respectively [17]. The TGA curves of PVDF-g-PGMA-g-PVPA(x) membranes showed a satisfactory thermal stability up to 210 °C. The initial weight loss at around 100 °C (approximately 1 %) can be attributed to the loss of loosely bound water (or moisture) that was possibly absorbed during storage. There was a small weight loss (approximately 5 %) between 140 and 180 °C due to condensation of phosphonic acid units of PVPA-side chains. After 275 °C, a remarkable weight loss in a single step originated from thermal decomposition of PGMA while PVPA started to decompose at around 420 °C. Finally, the final weight loss region occurs at 490 °C due to decomposition of PVDF backbone. Clearly, the dried materials are thermally stable up to at least 210 °C, after which, they decompose. Finally, it can be suggested that the obtained membranes can be used for testing in high temperature PEMFCs operation up to 200 °C.

Water uptake measurements

The water uptake is closely related to the efficieny of the fuel cells and basic properties of the membranes such as proton conductivity, mechanical property and stability. It plays an

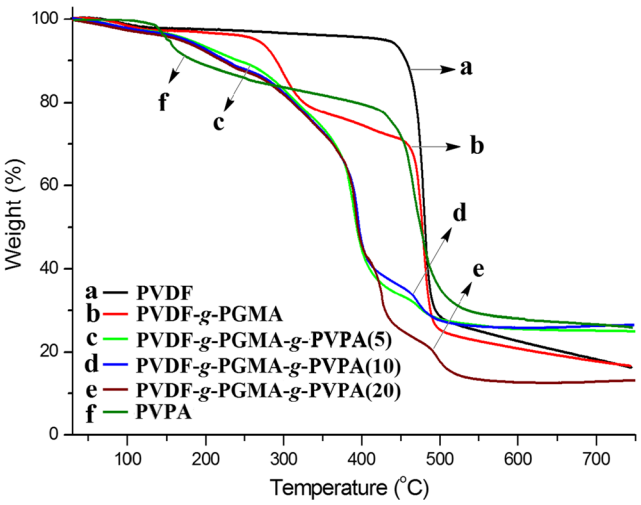

Fig. 7 TG thermograms of (**a**) original PVDF, (**b**) PVDF-*g*-PGMA, (**c**) PVDF-*g*-PGMA-*g*-PVPA(5), (**d**) PVDF-*g*-PGMA-*g*-PVPA(10), (**e**) PVDF-*g*-PGMA-*g*-PVPA(20) membranes, and (**f**) PVPA homopolymer at a heating rate of 10 °C/min in inert atmosphere

essential role in the membrane behavior which affects a large extent the proton conductivity depends the amount of water absorbed and even the proton conducting mechanism is influenced by it. Thus, the suitable water uptake is necessary. The water uptake measurements were made according to the literature [57]. The water uptake of the membranes were measured at room temperature under immersion in deionized water. Water uptakes of the PVDF-*g*-PGMA-*g*-PVPA(x) membranes are represented in Fig. 8. Generally, the water uptake increases with increasing hydrophilicity of the polymers. As can be seen from Fig. 8, water uptake increased with increasing of PVPA content because of swelling and hydrophilic properties of PVPA in the graft copolymer membranes. The highest water uptake values are listed in Table 3. As anticipated, the water uptake values decreased monotonously with increasing hydrophobic block size of the membranes. For instance, PVDF-*g*-PGMA-*g*-PVPA(5) membrane consisting the longest hydrophobic block showed relatively lower water uptakes of 28 wt %. PVDF-*g*-PGMA-*g*-PVPA(20) membrane has the highest water uptake value (225 %). Clearly, the results demonstrated that the increasing of PVPA content in PVDF-*g*-PGMA-*g*-PVPA(x) membranes enhanced the water uptake, and brought about better hydrophilicity.

Methanol permeability

The methanol permeability of PEMs is an important property in direct methanol fuel cells. But, it is a possible problem in the application of the membranes in fuel cells. The membranes with low methanol diffusion coefficient are required because methanol diffuses from the anode side to the cathode side leads to lower cell voltage and decreases fuel efficieny due to polarization losses. In this study, methanol permeability of the composite membranes was measured by simple home-made diaphragm diffusion cell similar to the study of Gasa et al. [58]. The cell was filled with 2 mL methanol and the mass flow was recorded as a function of time (Fig. 9). Molar methanol flux (J) through PVDF-*g*-PGMA-*g*-PVPA(x) membranes was calculated using Eq. (3). Methanol permeability of the graft copolymer membranes may be calculated using molar flux (J) shown in Eq. (4) [59, 60].

$$J = \frac{W}{M_W \times A \times t} \tag{4}$$

$$\frac{J_1 l_1}{J_2 l_2} = \frac{P_1}{P_2} \tag{5}$$

where J: flux, MW: molecular weight, W: weight loss (g), P: permeability, l: thickness (cm), A: area (cm^2), t: time (s).

As seen in the equations, the permeability is directly proportional to the molar flux. The molar flux of the PVDF-*g*-PGMA-*g*-PVPA(x) membranes are depicted in Fig. 9. The values are 3.12×10^{-9}, 2.78×10^{-9} and 2.28×10^{-9} mol cm^{-2} s^{-1}, respectively, for PVDF-*g*-PGMA-*g*-PVPA(5), PVDF-*g*-PGMA-*g*-PVPA(10), PVDF-*g*-PGMA-*g*-PVPA(20) membranes. Previously, the methanol permeability of Nafion 112 in the same conditions was determined as 1.89×10^{-9} mol cm^{-2} s^{-1} [59]. As seen in Fig. 9, the methanol permeability of the membranes are very close to Nafion 112. This means that the PVDF-*g*-PGMA-*g*-PVPA(x) membranes might be prospective to be used as a canditate of Nafion in PEMFCs.

X-ray diffraction (XRD)

X-ray diffractometry measurements were carried out to investigate the structural changes induced by the introduction of PGMA grafts to the PVDF films and subsequent followed grafting of the obtained PVDF-*g*-PGMA membranes with PVPA homopolymer. Figure 10 represents the XRD pattern of original PVDF, PVDF-*g*-PGMA, and PVDF-*g*-PGMA-*g*-

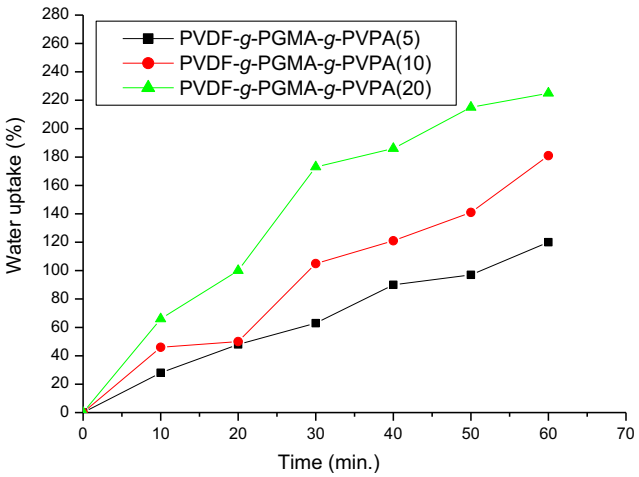

Fig. 8 Water uptakes of PVDF-*g*-PGMA-*g*-PVPA(x) (x=5, 10, 20 wt %) membranes at the time of 10–60 min in deionized water at 25 °C

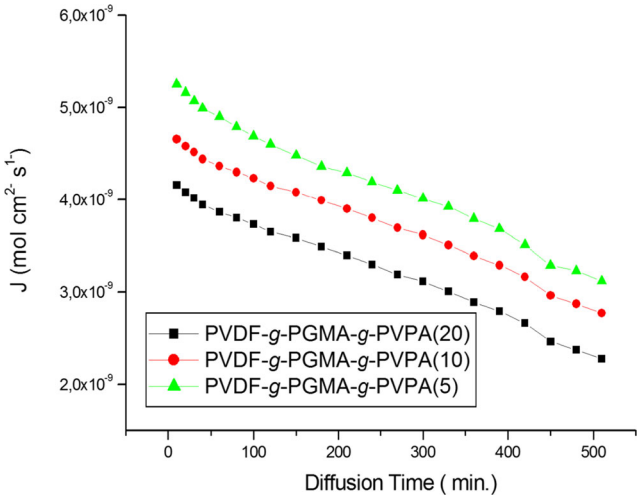

Fig. 9 Methanol permeability of PVDF-*g*-PGMA-*g*-PVPA(x) membranes

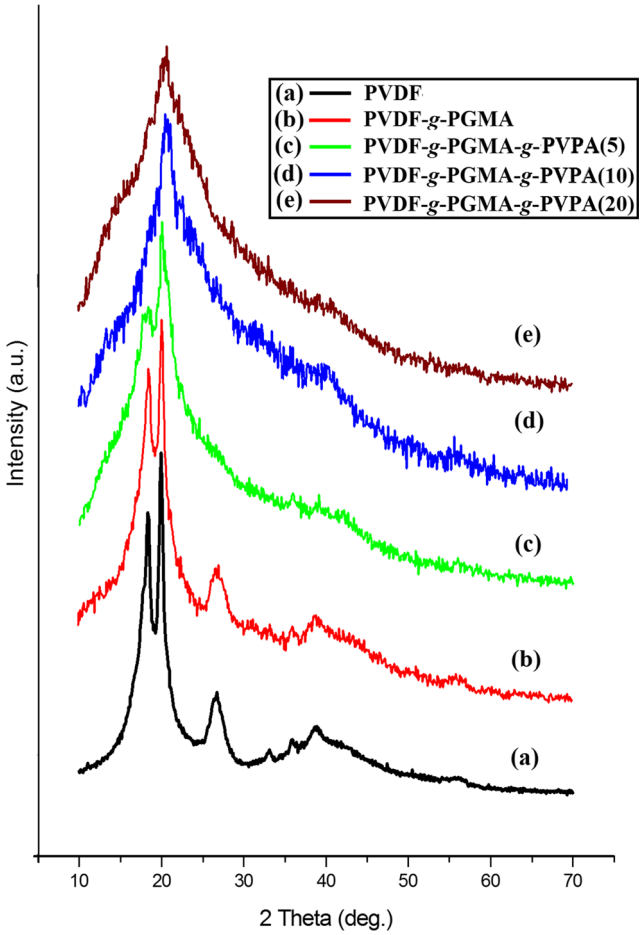

Fig. 10 XRD patterns of (**a**) PVDF, (**b**) PVDF-*g*-PGMA, (**c**) PVDF-*g*-PGMA-*g*-PVPA(5), (**d**) PVDF-*g*-PGMA-*g*-PVPA(10), (**e**) PVDF-*g*-PGMA-*g*-PVPA(20) membranes

PVPA(x) membranes. PVDF is a polymorphic, semi-crystalline polymer which are primarily four kinds of crystal structures such as α, β, γ, δ, wherein α type and β type are the main crystal structures of PVDF [18, 61–63]. The peak obtained at around 2θ=18.7°, 20.0°, and 26.4° reflect α-crystal structure which can be indexed α (020), α (110) and α (021) for pure PVDF. The peaks at 2θ=34.8° and 36.2° relate to the (200) plane of α-phase of PVDF and the peak at 2θ=39.2° refers to the combined (201) and (111) reflections of the β-phase due to molecular defects caused by head-head and tail-tail sequences [18, 64, 65]. After grafting of PGMA onto alkaline treated PVDF, the crystallinity of PVDF-*g*-PGMA graft copolymer (Fig. 10b) did not undergo any changes. The position of peaks is almost similar to those observed in alkaline treated PVDF. There was no additional phase detected in the PVDF matrix due to chemical modifications which means PGMA chains were grafted only on the surface of PVDF [66]. For PVDF-*g*-PGMA-*g*-PVPA(5) membrane, the characteristic peak at around 26.4° which can be indexed α (021) almost disappeared immediately. In addition, the peak at around 2θ=18.7° which can be indexed α (020) almost cleared instantly. The peaks at 2θ=26.4°, 34.8° and 36.2° relate to the (021) and (200) planes of α-phase of PVDF and the peak at 2θ=39.2° refers to the combined (201) and (111) reflections of the β-phase due to molecular defects caused by head-head and tail-tail sequences [18, 64, 65] were keenly destructed as can be seen in Fig. 10d and e. These results showed that the original crystalline structure of pure PVDF and PVDF-*g*-PGMA graft copolymer was seriously destroyed. As can be seen from XRD curves, when the PVPA content was increased, the amorphous nature of the PVDF-*g*-PGMA-*g*-PVPA(x) membranes increased [3, 5, 66] and the crystallinity of the membranes decreased. This behavior might have been explained as the elimination of hydrogen bonding network between epoxy rings of PVDF-*g*-PGMA graft copolymer and phosphonic acid units of PVPA at higher acid compositions. Because of the crystallite size that determined nearly 5.0±2.0 nm by using Scherrer's equation. The results are summarized in Table 2.

Atomic force microscopy (AFM)

AFM was used for the determination of phase morphology, heterogeneity, or homogeneity of the membranes. Moreover, the surface roughness of the membranes was determined. The changes in surface topography of the alkaline-treated PVDF after each modification (grafting) steps were measured up by AFM. Figure 11 displays the representative AFM height images of the alkaline treated-PVDF and functionalized PVDF membrane surfaces with scanned areas of 10×10 μm which were obtained at a resolution of 512×512 points within the range of 0.5–0.8 Hz scan rate and were subjected to first-order flattening. Surface roughness was calculated by using the Root Mean Square (RMS) (eq. 1), that is, the standard deviation of the Z values within a given area, where Zave is the average, Zi is the current Z value, and N is the number of points within the analyzed area. It was noted that the surface roughness depends on the curvature and size of the AFM tip and on the image processing. The RMS mean values and the standard deviations were obtained by analyzing at least 8

Table 2 The mean RMS roughness values with the standard deviations and the crystallite size of PVDF, PVDF-*g*-PGMA graft copolymer, and PVDF-*g*-PGMA-*g*-PVPA(x) membranes

Samples	Roughness (nm)[a]	crystallite size (nm)[b]
PVDF	50.24±8.16	5.0±2.0
PVDF-*g*-PGMA	193.12±27.75	4.5±0.6
PVDF-*g*-PGMA-*g*-PVPA(5)	100.05±13.88	3.2±0.4
PVDF-*g*-PGMA-*g*-PVPA(10)	64.33±8.88	2.8±0.3
PVDF-*g*-PGMA-*g*-PVPA(20)	26.78±5.06	1.8±0.5

[a] calculated from AFM

[b] calculated from XRD

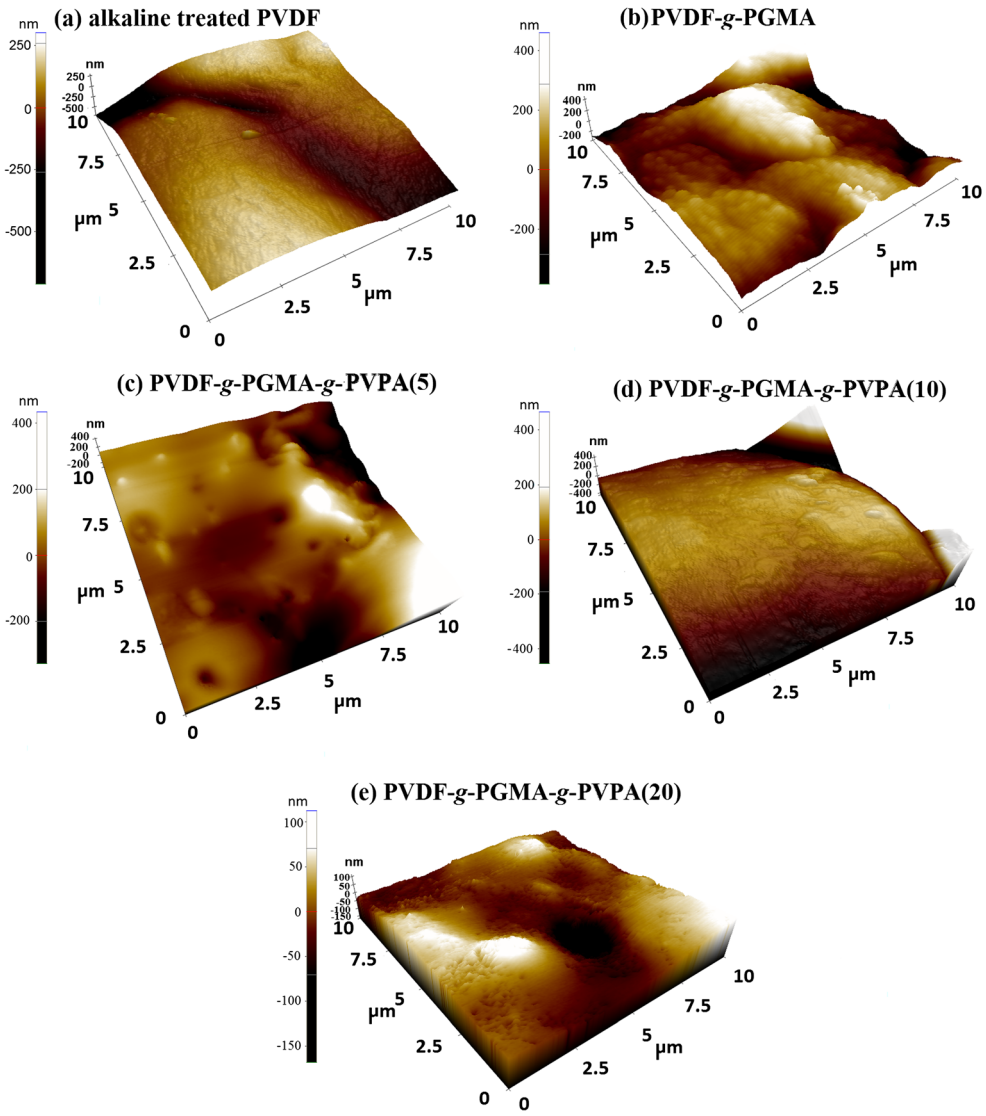

Fig. 11 Surface topography determined by representative AFM images of the (**a**) alkaline-treated PVDF, (**b**) PVDF-*g*-PGMA surface, (**c**) PVDF-*g*-PGMA-*g*-PVPA(5) surface, (**d**) PVDF-*g*-PGMA-*g*-PVPA(10) surface, and (**e**) PVDF-*g*-PGMA-*g*-PVPA(20) surface. The root-mean-squared (RMS) surface roughness of the different PVDF based membranes was obtained over a scan size of 10×10 μm

AFM images. The mean values of surface roughness of alkaline treated PVDF and functionalized PVDF membranes are listed in Table 2.

The alkaline-treated PVDF is relatively uniform and smooth with the root-mean-square (RMS) surface roughness values of about 50.24 nm (Fig. 11b). Upon grafting of PGMA, the surface roughness of PVDF-*g*-PGMA membrane reveals an obvious increase about 193.12 nm. This result was consistent with the previous findings that the grafting of the PGMA can lead to a significant increase in surface roughness value, as well as surface morphology [67]. After grafting of PVDF-*g*-PGMA copolymer with PVPA, by increasing the PVPA ratio, it was noticed a considerable decreasing of the surface roughness from 100.05 to 26.73 nm. The immobilization of PVPA can contract the PGMA domains on the PVDF surface, thus resulting in a further decrease in the surface roughness. Furthermore, the images exhibit single phase formation and the membranes seem homogeneous at nanometer-scale level except of image (b). As a consequence, the surface topography measured by AFM is an alternative way to ascertain successful modification of PVDF.

Morphology

Surface morphologies of the membranes were systematically analyzed using scanning electron microscopy (SEM) and the images of alkaline treated PVDF, PVDF-*g*-PGMA, and PVDF-*g*-PGMA-*g*-PVPA(x) membranes are represented in Fig. 12. There is formation of a smooth surface of the alkaline-treated PVDF powder and a number of pores appear as depicted in Fig. 12a [23, 61, 67–70]. Upon grafting of PGMA onto the alkaline treated PVDF, the surface morphology of PVDF films becomes rougher than that of the alkaline treated PVDF surface. It has a much more uniform pore size

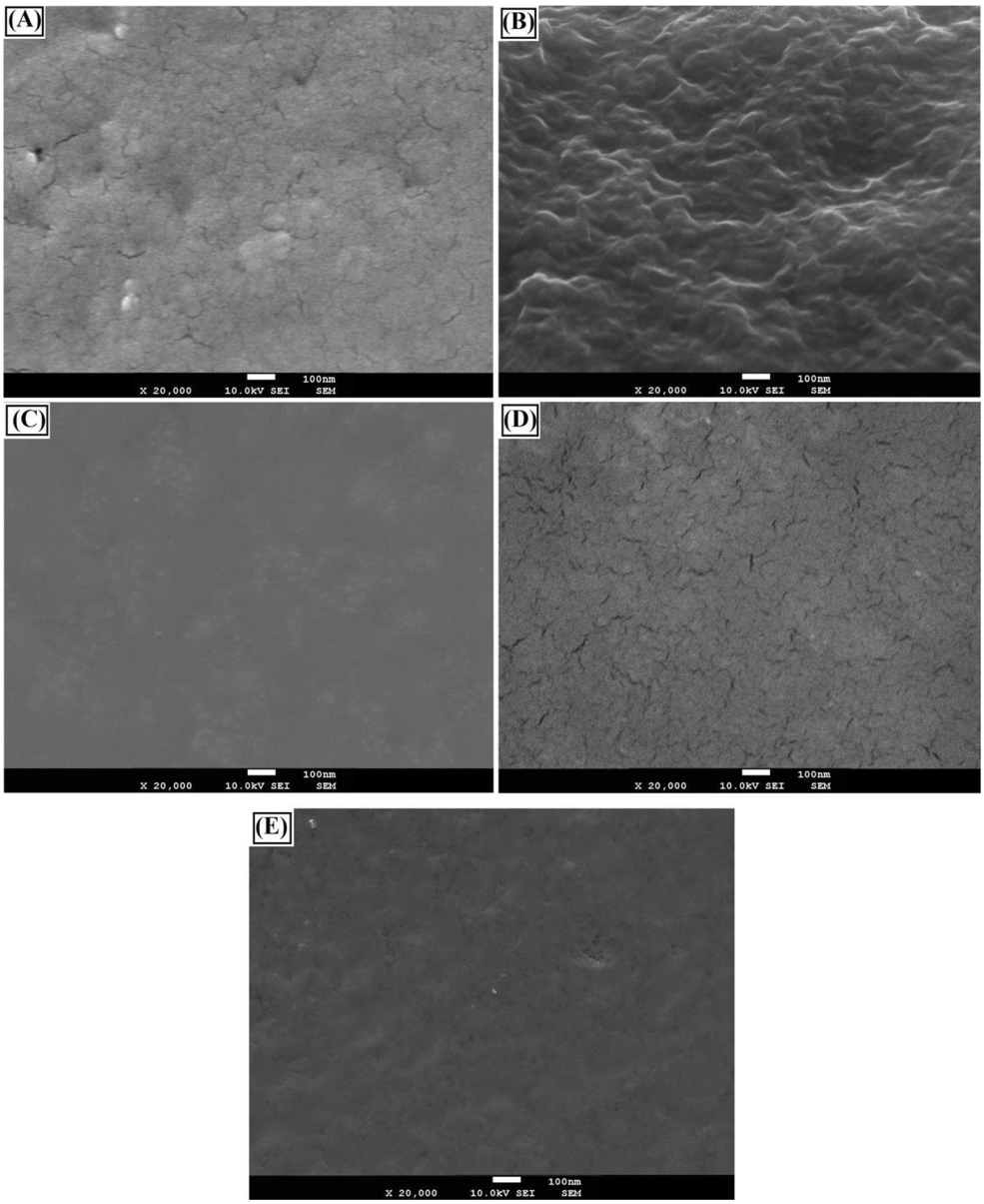

Fig. 12 SEM images of the surface of (**a**) alkaline-treated PVDF powder, (**b**) PGMA-grafted PVDF (PVDF-*g*-PGMA), (**c**) PVDF-*g*-PGMA-*g*-PVPA(5), (**d**) PVDF-*g*-PGMA-*g*-PVPA(10), and (**e**) PVDF-*g*-PGMA-*g*-PVPA(20) graft copolymer membranes at 100 nm scale level by 20,000× magnification, respectively

distribution and a higher degree of porosity, induced by the PGMA graft chains, than those of the alkaline treated PVDF. It is presented that the image (B) exhibits uniform and porous structure. It is clear from the image (B) that no phase separation has been observed upon grafting step. It is also clear that no cracks were observed which indicates homogeneity of the grafting process. These results confirmed that GMA monomer is grafted onto the PVDF [67–69]. After modification of PVDF-*g*-PGMA copolymer with PVPA, we observed that all samples (Fig. 12c-e) were homogeneously dissipated with increasing the PVPA content and the images showed single phase formation due to strong interaction between phosphonic acid groups of PVPA and epoxy units of PVDF-*g*-PGMA. In all samples (Fig. 12c-e), the images showed single phase formation. This result demonstrated that there was no agglomeration or phase separation at the nanometer level. As a result, these results are well consistent with those from the observation of AFM images.

Proton conductivity measurements

The proton conductivity of PEM is the crucial factor to be investigated for the potential application in high temperature proton exchange membrane fuel cells. The design and development of high performance PEMs with high proton conductivity in anhydrous conditions have been fascinated.

The proton conductivity of PVDF-*g*-PGMA-*g*-PVPA(20) membrane is shown in Fig. 13 as a function of temperature. At lower frequency regions, the conductivity increases with log frequency then leveled off which is due to electrode

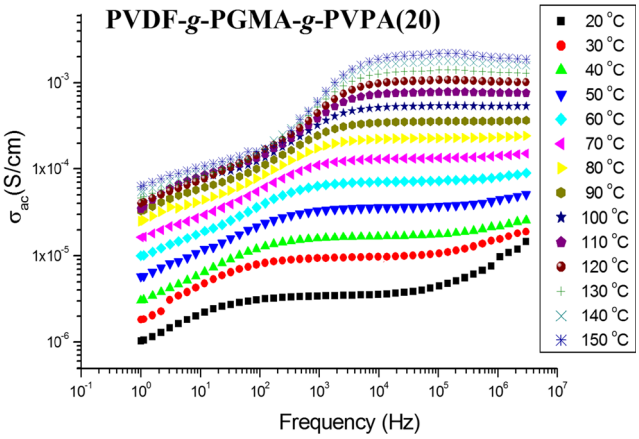

Fig. 13 AC conductivity versus frequency of PVDF-*g*-PGMA-*g*-PVPA(20) membrane at several temperatures

polarizations. The irregularities at the low frequency side correspond to polarization blocking the electrode-electrolyte interface and the conductivity increases at low temperature and high frequencies results from the regular dispersion in polymer electrolytes [3, 5, 6]. Membrane with higher PVPA content exhibit the highest proton conductivity due to the higher concentration of protons arising from the acidic groups of PVPA. Furthermore, the proton conductivity rises with temperature due to the higher proton mobility, as expected. Maximum proton conductivities of the obtained PEMs are listed in Table 3. In the anhydrous conditions, the highest proton conductivity of PVDF-*g*-PGMA-*g*-PVPA(20) was found as 0.0023 Scm^{-1} at 150 °C.

The temperature dependence of the proton conductivities of the PVDF-*g*-PGMA, PVDF-*g*-PGMA-g-PVPA(x) membranes, PVPA homopolymer, and Nafion 117 were compared in Fig. 14 and the values were listed in Table 3. It can be seen that the proton conductivity display a linear dependence on the temperature and PVPA content. Generally, the DC curve can be explained with Arrhenius or Vogel-Tamman-Fulcher (VTF) behavior depending on the type of the curve where during the measurement temperature range no T_g was observed and there is no change in linearity of DC curve (Fig. 14). Herein, the curves are close to linearity. Therefore, we can say that the PVPA, PVDF-*g*-PGMA, and PVDF-*g*-PGMA-*g*-PVPA(x) membranes show Arrhenius behavior in the measurement range [5, 6]. It can be explained with the Arrhenious equation:

$$\ln \sigma = \ln \sigma_0 - E_a / kT \quad (6)$$

where σ_0 is the pre-exponential terms, E_a is the activation energy, and k is the Boltzmann constant.

PVDF has a similar backbone with Nafion and it provided a high thermally and mechanically stable matrix and good film formability. PVPA is an acidic polymer. It has high proton conductivity (10^{-3} Scm^{-1}) and good film forming property, which are important characteristics of a polymer electrolyte membrane [6, 39, 40]. Although pure PVPA has several advantages, its water solubility makes it an improper material for PEMFC applications. Previously, Sen et al. reported the preparation of PVPA blended Nafion, Nafion-$P(VPA)_3$, with a maximum proton conductivity of 1.1×10^{-5} S/cm at 130 °C and anhydrous conditions [71]. In another work reported by Aslan et al. a maximum proton conductivity of 5×10^{-5} S/cm at 150 °C was found for PVPA-grafted poly(glycidylmethacrylate), P(GMA)-*g*-$P(VPA)_{10}$ [41]. In the present study, the highest maximum proton conductivity of PVDF-*g*-PGMA-*g*-PVPA(20) membrane was measured as 0.0023 Scm^{-1} at 150 °C, a superior conductivity value as compared to the afore-mentioned ones.

In our study, PVPA provides a hydrophilic channel in PVDF-*g*-PGMA-*g*-PVPA(x) membranes similar to Nafion. Herein, the proton conductivity of the membranes is improved with PVPA content and maximum conductivity was observed for PVDF-*g*-PGMA-*g*-PVPA(20) membrane. These results showed that in PVDF-*g*-PGMA-*g*-PVPA(x) systems, the PVPA composition is highly effective on the proton conductivity of the membranes. PVPA interacts with PGMA units of

Table 3 Water uptake, methanol permeability, and maximum proton conductivity values of the obtained PVDF based membranes

Sample	Water uptake (%)	Methanol permeability (mol cm^{-2} s^{-1})	Relative humidity (%)	Max. proton conductivity (Scm^{-1})
PVDF	–	–	–	–
PVDF-*g*-PGMA	–	–	-	2.39×10^{-7} Scm^{-1} at 150 °C
PVDF-*g*-PGMA-*g*-PVPA(5)	–	–	50	0.024 Scm^{-1} at 100 °C
PVDF-*g*-PGMA-*g*-PVPA(5)	121	3.12×10^{-9}	–	6.44×10^{-5} Scm^{-1} at 150 °C
PVDF-*g*-PGMA-*g*-PVPA(10)	–	–	50	0.031 Scm^{-1} at 100 °C
PVDF-*g*-PGMA-*g*-PVPA(10)	181	2.78×10^{-9}	–	8.51×10^{-4} Scm^{-1} at 150 °C
PVDF-*g*-PGMA-*g*-PVPA(20)	–	–	50	0.034 Scm^{-1} at 100 °C
PVDF-*g*-PGMA-*g*-PVPA(20)	225	2.28×10^{-9}	–	0.0023 Scm^{-1} at 150 °C
PVPA	–	–	–	1.51×10^{-3} Scm^{-1} at 150 °C
Nafion 117	–	1.89×10^{-9}	–	2.95×10^{-5} Scm^{-1} at 150 °C

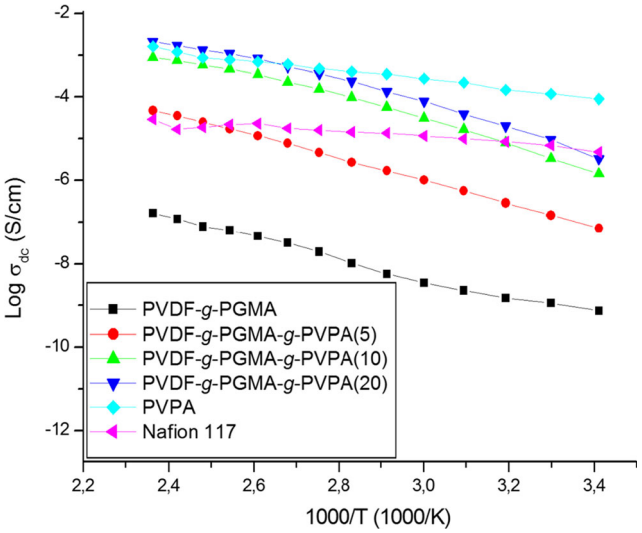

Fig. 14 Variation of the DC proton conductivity of Nafion 117, PVPA, PVDF-*g*-PGMA, and PVDF-*g*-PGMA-g-PVPA(x) membranes as a function of reciprocal temperature

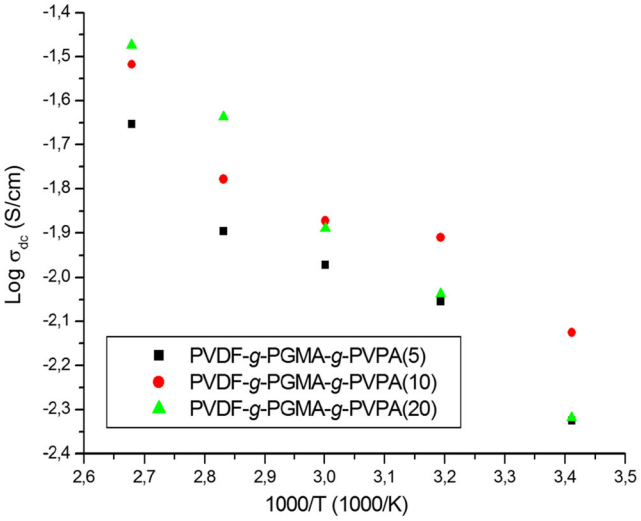

Fig. 15 The effect of PVPA content on DC proton conductivities of 50 % humidified PVDF-*g*-PGMA-*g*-PVPA(x) membranes as a function of reciprocal temperature

PVDF-*g*-PGMA backbone and the major part of proton transport is provided over the phosphonic acid phase.

Furthermore, the importance of membrane's quality on proton conductivity is further underscored from the comparison between SEM images and the measured proton conductivities. It is evident from Fig. 12 that the morphologies of the membranes seem to be smoothness. The smoothness of the membranes, which indicating formation of continuous conducting channels essential for enhancement of proton conductivity, increases with the increment of PVPA content in the PVDF-*g*-PGMA-*g*-PVPA(x) systems. PVDF-*g*-PGMA-*g*-PVPA(20) showed the smoothest surface and the highest proton conductivity [72].

The proton conductivity was investigated also in humidified condition and illustrated in Fig. 15. The proton conductivity values generally depend on both temperature and water at humidified conditions. Previously, the temperature dependence of proton conductivity of Nafion 117 at various humidity levels was studied [73, 74]. Previously, the proton conductivity of Nafion117 at 50 % relative humidity was measured as 0.03 S/cm at 40 °C [73]. In our study, similar to anhydrous systems at high temperature, maximum proton conductivity was measured for the sample with x=20. In the relative humidity (RH=50 %), the highest maximum proton conductivity of PVDF-*g*-PGMA-*g*-PVPA(20) membrane was found as 0.023 S/cm at 80 and 0.034 at 100 °C.

Cyclic voltammetry

Cyclic voltammogram of PVDF-*g*-PGMA-*g*-PVPA(20) membrane was given in Fig. 16. The measurement was performed in a typical three electrode cell containing 0.1 mol dm^{-3} CH_3CN solution of tetrabutylammonium chloride (TBACl) using a platinum work electrode, a platinum auxiliary electrode, and an Ag/Ag^+ reference electrode. The voltammogram shows that the graft copolymer membrane comprises no peak within in the anodic and cathodic sweep (−1.5 to 1.5 V potential range). Thus the electrochemical stability window is about 3 V. These results implied that the PVDF-*g*-PGMA-*g*-PVPA(20) membrane had adequate electrochemical stability under fuel cell conditions.

Conclusions

In this study, we have fabricated novel PEMs consisting of PVDF membranes, with PVPA functional-poly(glycidyl methacrylate) (PGMA) side chains (PVDF-*g*-PGMA-*g*-PVPA(x)), for application in PEMFCs. Herein, alkaline

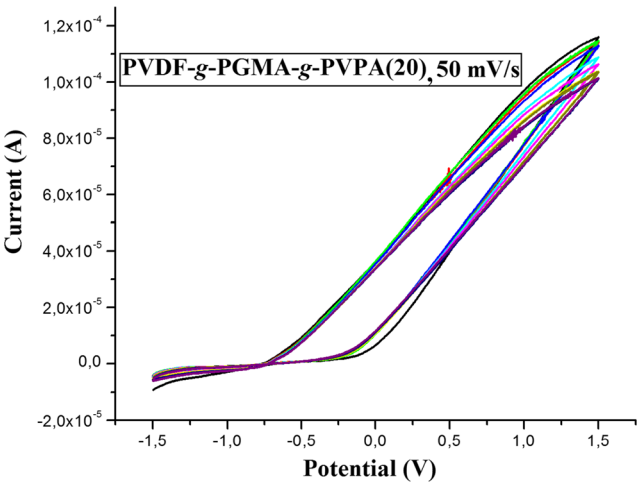

Fig. 16 Cyclic voltammograms of PVDF-g-PGMA-g-PVPA(20) in 0.1 M TBACl / acetonitrile. Curves were obtained with a scan rate of 50 mV/s

treated PVDF was used as a macromolecule in conjunction with GMA in the graft copolymerization using a simple "grafting through" approach. Novel PEMs were synthesized via free radical-initiated graft copolymerization of glycidyl methacrylate (GMA) from alkaline-treated PVDF backbone, followed by reaction of the oxirane rings in the GMA side chains with PVPA, eventually fabricating various PVDF-*g*-PGMA-*g*-PVPA(x) membranes. The FTIR and ^{1}H-NMR results confirmed the successful tethering of the PGMA polymer chains onto PVDF. ^{1}H-NMR results showed grafting efficiency of 80.62 wt % for PVDF-*g*-PGMA graft copolymers. TGA showed that the PVDF-*g*-PGMA and PVDF-*g*-PGMA-*g*-PVPA(x) membranes were thermally stable up 275 and 210 °C, respectively. Methanol permeability experiments exhibited that the obtained graft copolymer membranes have similar methanol permeability values with Nafion 112. The XRD analysis divulged the crystallinity of the obtained membranes. After grafting of PGMA onto alkaline treated PVDF, the crystallinity of PVDF-*g*-PGMA did not undergo any changes. The XRD results showed that the amorphous nature of the obtained membranes, PVDF-*g*-PGMA-*g*-PVPA(x), increases with the increasing amount of PVPA. The proton conductivities of the membranes were measured by using impedance dianalyzer. The maximum proton conductivity was found for PVDF-*g*-PGMA-*g*-PVPA(20) with a degree of grafting of 80.62 % as 0.0023 S/cm at 150 °C in anhydrous condition. The proton conductivity of the same material was measured as 0.034 at 100 °C with *RH*=50 %. In that study, PVPA has high contribution to the proton conduction and the sample with the highest PVPA content, PVDF-*g*-PGMA-*g*-PVPA(20), has considerable conductivity in the humidified condition and low methanol permeability. This study presents the fabrication of novel PEMs by the use of alkaline treated PVDF and GMA monomer in a "grafting through" strategy which can be interesting for designing further membranes for fuel cells, since the method offers an easy and versatile fabrication of PEMs with relatively high grafting efficiencies and high proton conductivities both anhydrous and humidified (*RH*=50 %) conditions. Furthermore, the obtained membranes may a suitable candidate to be employed in fuel cells.

Acknowledgments This research has been supported by Yildiz Technical University Scientific Research Projects Coordination Department with Project number 2014-07-01-KAP02. We would like to thank Fatih University-BINATAM center for the SEM-EDS, XRD and AFM measurements. We would also like to thank Mr. Ibrahim Sasmaz for measuring the NMR spectra at Fatih University.

References

1. Sen U, Usta H, Acar O, Citir M, Canlier A, Bozkurt A, Ata A (2015) Macromol Chem Phys 216:106–112
2. Tang QW, Yuan S, Cai H (2013) J Mater Chem A 1:630–636
3. Sinirlioglu D, Celik SU, Muftuoglu AE, Bozkurt A (2014) Macromol Chem Phys 215:269–279
4. Tang QW, Cai H, Yuan S, Wang X, Yuan W (2013) Int J Hydrog Energy 38:1016–1026
5. Sinirlioglu D, Celik SU, Muftuoglu AE, Bozkurt A (2015) Polym Eng Sci 55:260–269
6. Celik SU, Bozkurt A, Hosseini SS (2012) Prog Polym Sci 37:1265–1291
7. Parvole J, Jannasch P (2008) Macromolecules 41:3893–3903
8. Celik SU, Akbey U, Bozkurt A, Graf R, Spiess HW (2008) Macrom Chem Phys 209:593–603
9. Zhao Z, Pu H, Chang Z, Pan H (2014) Int J Hydrog Energy 39: 6657–6663
10. Singha S, Jana T (2014) Polymer 55:594–601
11. Wang SH, Lin HL (2014) J Power Sources 257:254–263
12. Sinirlioglu D, Celik SU, Muftuoglu AE, Bozkurt A (2014) J Appl Polym Sci 131:40107
13. Das S, Kumar P, Dutta K, Kundu PP (2014) Appl Energy 113:169–177
14. Kim DS, Robertson GP, Kim YS, Guiver MD (2009) Macromolecules 42:957–963
15. Lin H, Zhao C, Cui Z, Ma W, Fu T, Na H, Xing W (2009) J Power Sources 193:507–514
16. Jouanneau J, Mercier R, Gonon L, Gebel G (2007) Macromolecules 40:983–990
17. Arslantas A, Sinirlioglu D, Eren F, Muftuoglu AE, Bozkurt A (2014) J Polym Res 21:437
18. Sinirlioglu D, Muftuoglu AE, Golcuk K, Bozkurt A (2014) J Polym Sci A Polym Chem 52:1885–1897
19. Sasa D, Sinirlioglu D, Muftuoglu AE, Eren F, Celik SU, Bozkurt A (2013) J Polym Res 20:313
20. Abdel-Hady EE, El-Toony MM, Abdel-Hamed MO (2013) Electrochim Acta 103:32–37
21. Golcuk S, Muftuoglu AE, Celik SU, Bozkurt A (2013) J Polym Res 20:144
22. Sezgin S, Sinirlioglu D, Muftuoglu AE, Bozkurt A (2014) J Chem 2014:963131
23. Lepit A, Aini NA, Jaafar NK, Hashim N, Ali AMM, Dahlan KZM, Yahya MZA (2012) Int J Electrochem Sci 7:8560–8577
24. Li L, Yu Y, Deng B, Ji Y, Yu Y, Leidong X, Jingye L, Ming Y (2011) Nucl Sci Tech 22:160–165
25. Li L, Deng B, Ji Y, Yu Y, Xie L, Li J, Lu X (2010) J Memb Sci 346: 113–120
26. Shamsaei E, Saidi H, Nasef MM, Kuala L, Yahaya AH (2014) Radiochim Acta 102:351–362
27. Meng JQ, Chen CL, Huang LP, Du QY, Zhang YF (2011) Appl Surf Sci 257:6282–6290
28. Sui Y, Wang Z, Gao X, Gao C (2012) J Membr Sci 413:38–47
29. Roh DK, Ahn SH, Seo JA, Shul YG, Kim JH (2010) J Polym Sci B Polym Phys 48:1110–1117
30. Kim YW, Choi JK, Park JT, Kim JH (2008) J Membr Sci 313:315–322
31. Kim YW, Park JT, Koh JH, Roh DK, Kim JH (2008) J Membr Sci 325:319–325
32. Kim YW, Lee DK, Lee KJ, Kim JH (2008) Eur Polym J 44:932–939
33. Tang Z, Li W, Liu L, Huang L, Zhou J, Yu H (2009) Chin J Chem 27:419–422
34. Li S, Fried JR, Colebrook J (2013) Polym Eng Sci 53:597–608
35. Ye S, Pu H, Wan D (2012) Polym Eng Sci 52:1450–1456
36. Pu H, Wu J, Wan D, Chang Z (2008) J Membr Sci 322:392–399
37. Modestov AD, Tarasevich MR, Filimonov VY, Leykin AY (2009) J Electrochem Soc 156:B650–B656
38. Weber J, Kreuer KD, Maier J, Thomas A (2008) Adv Mater 20: 2595–2598
39. Yamada M, Honma I (2005) Polymer 46:2986–2992

40. Kaltbeitzel A, Schauff S, Steininger H, Bingol B, Brunklaus G, Meyer WH, Spiess HW (2007) Solid State Ion 178:469–474
41. Aslan A, Celik SU, Bozkurt A (2009) Solid State Ion 180:1240–1245
42. Bingöl B, Meyer WH, Wagner M, Wegner G (2006) Macromol Rapid Commun 27:1719–1724
43. Ross GJ, Watts JF, Hill MP, Morrissey P (2000) Polymer 41:1685–1696
44. Bottino A, Capannelli G, Monticelli O, Piaggio P (2000) J Membr Sci 166:23–39
45. Liu DM, Chen YW, Zhang N, He XH (2006) J Appl Polym Sci 101: 3704–3712
46. Nanjundan S, Unnithan CS, Selvamalar CSJ, Penlidis A (2005) React Funct Polym 62:11–24
47. Tan S, Li J, Gao G, Li H, Zhang Z (2012) J Mater Chem 22:18496–18504
48. Tan S, Hu X, Ding S, Zhang Z, Li H, Yang L (2013) J Mater Chem A 1:10353–10361
49. Cheburkov Y, Moore GGI (2003) J Fluor Chem 123:227–231
50. Yang ZY (2003) J Org Chem 68:5419–5421
51. Lu YY, Claude J, Zhang QM, Wang Q (2006) Macromolecules 39: 6962–6968
52. Foris A (2004) Magn Reson Chem 42:534–555
53. Göktepe F, Celik SU, Bozkurt A (2008) J Non-Cryst Solids 354: 3637–3642
54. Sevil F, Bozkurt A (2004) J Phys Chem Solids 65:1659–1662
55. Celik SU, Bozkurt A (2008) Eur Polym J 44:213–218
56. Tang W, Zhu T, Zhou P, Zhao W, Wang Q, Feng G, Yuan H (2011) J Mater Sci 46:6656–6663
57. Huang YJ, Ye YS, Yen YC, Tsai LD, Hwang BJ, Chang FC (2011) Int J Hydrogen Energy 36:15333–15343
58. Gasa JV, Weiss RA, Shaw MT (2007) J Membr Sci 304:173–180
59. Sen U, Celik SU, Ata A, Bozkurt A (2008) Int J Hydrog Energy 33: 2808–2815
60. Boroglu MS, Celik SU, Bozkurt A, Boz I (2011) J Membr Sci 375: 157–164
61. Dong Z, Zhang Q, Yu C, Peng J, Ma J, Ju X, Zhai M (2013) Ionics 19:1587–1593
62. Zhang PY, Yang H, Xu ZL, Wei YM, Guo JL, Chen DG (2013) J Polym Res 20:66
63. Glaub B, Steinmann W, Walter S, Beckers M, Gunnar S, Gries T, Roth G (2013) Materials 6:2642–2661
64. Yu S, Zheng W, Yu W, Zhang Y, Jiang Q, Zhao Z (2009) Macromolecules 42:8870–8874
65. Huang XY, Jiang PK, Kim C, Liu F, Yin Y (2009) Eur Polym J 45: 377–386
66. Bach LG, Islam MR, Lee DC, Lim KT (2013) Appl Surf Sci 283: 546–553
67. He F, Luo B, Yuan S, Liang B, Choong C, Pehkoneni SO (2014) RSC Adv 4:105–117
68. Cai T, Neoh KG, Kang ET (2011) Langmuir 27:2936–2945
69. Young TH, Chang HH, Lin DJ, Cheng LP (2010) J Membr Sci 350: 32–41
70. Abu-Saied MA, Fontananova E, Drioli E, Mohy Eldin MS (2013) J Polym Res 20:187
71. Sen U, Acar O, Celik SU, Bozkurt A, Ata A, Tokumasu T, Miyamoto A (2013) J Polym Res 20:217
72. Nazir NA, Kim N, Iglesias WG, Jakli A, Kyu T (2012) Polymer 53: 196–204
73. Takimoto N, Wu L, Ohira A, Takeoka Y, Rikukawa M (2009) Polymer 50:534–540
74. Casciola M, Alberti G, Sganappa M, Narducci R (2006) J Power Sources 162:141–145